Journal of Orthopaedic Translation 43 (2023) 21–35

Contents lists available at ScienceDirect

Journal of Orthopaedic Translation

journal homepage: www.journals.elsevier.com/journal-of-orthopaedic-translation

Original Article

Silicone rubber sealed channel induced self-healing of large bone defects: Where is the limit of self-healing of bone?

Feng Gu [a], Ke Zhang [a], Wan-an Zhu [b], Zhenjiang Sui [a], Jiangbi Li [a], Xiaoping Xie [a], Tiecheng Yu [a,*,1]

[a] Department of Orthopedics, First Hospital of Jilin University, Changchun, 130021, China
[b] Department of Radiology, First Hospital of Jilin University, Changchun, 130021, China

ARTICLE INFO

Keywords:
Bone defect
Regeneration
Self-healing
Silicone rubber

ABSTRACT

Background: Large defects of long tubular bones due to severe trauma, bone tumor resection, or osteomyelitis debridement are challenging in orthopedics. Bone non-union and other complications often lead to serious consequences. At present, autologous bone graft is still the gold standard for the treatment of large bone defects. However, autologous bone graft sources are limited. Silicon rubber (SR) materials are widely used in biomedical fields, due to their safety and biocompatibility, and even shown to induce nerve regeneration.

Materials and methods: We extracted rat bone marrow mesenchymal stem cells (BMMSCs) in vitro and verified the biocompatibility of silicone rubber through cell experiments. Then we designed a rabbit radius critical sized bone defect model to verify the effect of silicone rubber sealed channel inducing bone repair in vivo.

Results: SR sealed channel could prevent the fibrous tissue from entering the fracture end and forming bone nonunion, thereby inducing self-healing of long tubular bone through endochondral osteogenesis. The hematoma tissue formed in the early stage was rich in osteogenesis and angiogenesis related proteins, and gradually turned into vascularization and endochondral osteogenesis, and finally realized bone regeneration.

Conclusions: In summary, our study proved that SR sealed channel could prevent the fibrous tissue from entering the fracture end and induce self-healing of long tubular bone through endochondral osteogenesis. In this process, the sealed environment provided by the SR channel was key, and this might indicate that the limit of self-healing of bone exceeded the previously thought.

The translational potential of this article: This study investigated a new concept to induce the self-healing of large bone defects. It could avoid trauma caused by autologous bone extraction and possible rejection reactions caused by bone graft materials. Further research based on this study, including the innovation of induction materials, might invent a new type of bone inducing production, which could bring convenience to patients. We believed that this study had significant meaning for the treatment of large bone defects in clinical practice.

1. Introduction

Large defects of long tubular bone caused by severe trauma, bone tumor resection and osteomyelitis debridement is a challenging orthopaedic problem [1,2]. In 1986, Schmitz JP proposed the concept of critical sized defects (CSD) [3] to indicate the threshold for self-healing of bone defects; it corresponds to a bone defect length exceeds 1.5 times of bone diameter. However, there is no clear and unified conclusion on this definition for humans. Some consider a length of human bone defect >50% of the diameter of the long tube bone or a length >2 cm large bone defect [4], while others consider only those >5 cm [5]. At present, autologous bone graft is the gold standard for the treatment of large defects of long tubular bones. However, autologous bone graft sources are limited. In addition, massive autologous bone grafts cause complications, such as nerve and vascular injury, infection, and chronic pain [6–8]. Accordingly, autologous bone grafting is often used for bone defects within 4–5 cm; for larger bone defects, this method often fails to achieve ideal repair [9,10]. In consequence, other methods are used for

* **Corresponding author**.
E-mail addresses: gufengjlu@163.com (F. Gu), zhangke_medical@163.com (K. Zhang), 448336550@qq.com (W.-a. Zhu), suizhenjiang2021@163.com (Z. Sui), lijb312@163.com (J. Li), xiexp20@mails.jlu.edu.cn (X. Xie), yutc@jlu.edu.cn (T. Yu).
[1] Present address: No. 1 Xinmin Street, Changchun City, Jilin Province, China

https://doi.org/10.1016/j.jot.2023.09.001
Received 13 May 2023; Received in revised form 2 August 2023; Accepted 12 September 2023

the repair and treatment of long tubular bone defects, including the Ilizarov technique (distraction osteogenesis) [11] and/or Masquelet technique, and bone tissue engineering [2,12,13]. However, the above methods have some issues. For instance, the Ilizarov technique requires a complex external fixator, and during distraction, the pressure on soft tissue often leads to continuous pain, while the risk of force line deviation, can cause infection and nerve injury [14–20]. On the other hand, the Masquelet technique induces the formation of an induction membrane through polymethyl methacrylate (PMMA) occupation followed by an autologous bone graft [21–25], resulting in a long treatment process, which also increases the uncertainty of the results [26]. Recently, bone tissue engineering has become a research hotspot. It requires seed cells, extracellular matrix scaffolds, and cytokines that promote growth, differentiation, and angiogenesis [27–31]. However, to date there is no technique or material available that completely solves the issues of large bone defects.

Bone is a composite structure including cells, extracellular matrix, and lipids [32]. About 20% of it is water, and the dry weight of bone is composed of 30%–35% organic matter and 65%–70% inorganic matter [33]. Bone tissue is one of the few tissues in the human body that can heal without scarring [34]. Fracture healing is a complex biological process involving multiple stages and under complex biological regulation. Bone healing requires numerous elements, the most important being osteoblast-related cells, bone conduction scaffolds, stable mechanical environment, and osteogenesis promoting growth factors. These four elements are also called the “diamond concept” of osteogenesis [35]. According to the process, bone healing can be indirect or direct [36]. Direct bone healing is uncommon in the natural state, and would occur only with anatomical reduction and complete stable fixation [36]. Indirect healing is the most important way of fracture healing, mainly including endochondral and intramembranous osteogenesis [37,38]. Intramembranous osteogenesis does not involve cartilage intermediates and mainly relies on direct differentiation of mesenchymal stem cells (MSCs) and neural crest cells [39], and mainly occurs in the regeneration of maxillofacial bones [40,41]. In contrast, endochondral osteogenesis requires a cartilaginous intermediate, and occurs primarily in the extremities, pelvis, and most axial skeleton, including the ribs, scapula, and skull base [39]. The first stage of bone healing is hematoma formation, immediately after trauma, involves peripheral blood, intramedullary blood cells, and intramedullary cells [36,42–44]. This process is accompanied by the development of an inflammatory response [45,46] that leads to hematoma coagulation between and around the fracture ends and formation of a precursor template for the intramedullary callus [47]. During the inflammatory response, MSCs undergo a process of selective migration to the injury site and continuously secrete various trophic factors, a function called “homing” [48–52]. Initial pro-inflammatory factors include tumor necrosis factor-α (TNF-α), interleukin-1 (IL-1), interleukin-6 (IL- 6), interleukin-11 (IL-11) and interleukin-18 (IL-18) [47]. Recruited MSCs and other cells gradually form a cartilage callus, which will be mineralized, resorbed, and gradually replaced by bone tissue during the subsequent osteogenesis [36]. Members of the transforming growth factor-β (TGF-β) family, including TGF-β1, TGF-β2, and TGF-β3, have been shown to play a very critical role in endochondral osteogenesis [36,53,54]; vascular endothelial growth factor (VEGF), platelet derived growth factor and fibroblast growth factor-2 (FGF-2) are also key mediators in this process [47,55]. In addition, the TGF-β gene can selectively induce and regulate the differentiation of MSCs into osteoblasts [56]. The initial hematoma at the fracture end and the subsequent acute inflammatory reaction resolve within a few days to a week after the fracture and are replaced by granulation tissue, which is rich in proliferating mesenchymal cells and forms neovascularization in the extracellular collagen matrix [34,36,57,58]. A few weeks after the injury, the cartilage eventually extends into the connecting fracture space, which, together with the accompanying fibrous tissue, is commonly referred to as a cartilage callus, providing initial mechanical stability to the fracture and acting as a scaffold for endochondral bone formation [34,36,57,58]. As chondrocytes proliferate, they become hypertrophic and enter the apoptotic phase, secreting calcium and angiogenesis-promoting components, and the extracellular matrix gradually begins to calcify; in this phase of hard callus formation, extensive vascularization of the cartilage occurs, and braided bone begins to deposit [34,36,47]. With the growth of the hard callus and braided bone, the fracture area is gradually filled with new bone and mechanical stability continuously increased. In the end, fracture healing enters the final shaping period. To increase the strength, bone tissue remodels into lamellar structures with medullary cavities during the shaping phase, in which osteoclasts play an important role [36,59–63].

Silicone rubber (SR) is a very important organosilicon product characterized by linear polymer polymerization with repeating silicon-oxygen (Si–O) bond as main chain and the side groups as organic groups. After vulcanization, it becomes an elastomer with a three-dimensional network structure [64]. SR material has good biocompatibility, good plasticity, stable chemical properties and is non-toxic, odorless, and not easily oxidized or denatured. Recently, some researchers have begun to use SR catheters to repair peripheral nerves [65–73]. Liao et al. used SR catheters to connect both ends of the sciatic nerve of SD rats treated with paclitaxel and combined electrical stimulation to achieve nerve regeneration [66], and Mohammadi et al. [74] used a matrix vascular block combined with a SR tube to repair the sciatic nerve in rats. Despite all the above evidence in the field of nerve regeneration, there are few reports on its application to bone defects. Researchers used SR temporary filling and bone grafting for repairing mandibular defects in previous study [75]. In the field of Neurosurgery, SR was used to prevent adhesion when skull defects exist [76]. SR was used in both skull and mandibular defects, so we believed that SR materials also had great potential for application and research value in long tubular bone defects. Based on Masquelet technology, this study utilized a SR sealed channel without bone grafting for the induction and repair of large defects of long tubular bones in vivo and in vitro.

2. Materials and methods

2.1. Animals

3-week-old male SD rats were selected for cell extraction. In addition, 6-month-old New Zealand white rabbits were used for this study. The experimental animals were divided into three groups: SR sealed channel group (SR group), SR channel group with holes (SR + Holes group) and blank Control group (Control group). The rabbits were sacrificed at eight time points (1 day, 3 days, 7 days, 14 days, 4 weeks, 8 weeks, 12 weeks, and 16 weeks). Six rabbits from each group were sacrificed at each time point.

2.2. BMMSC isolation and culture

3-week-old male SD rats were sacrificed and subsequently soaked in 75% alcohol for 30 min to isolate the primary cells. The rats' tibias and femora were collected for bone marrow mesenchymal stem cell (BMMSC) isolation. The bone marrow cavities were repeatedly flushed with Dulbecco's Modified Eagle Medium/F-12 (DMEM/F-12) (Gibco, Rockville, MD, USA), with 10% fetal bovine serum (FBS, Biological Industries, Israel) into 10-cm dishes using a syringe. Then, the bone marrow was incubated at 37 °C in 95% humidified air containing 5% CO_2 in DMEM/F-12 medium supplemented with 10% fetal bovine serum (FBS, Biological Industries, Israel). The culture medium was changed for the first time at 72 h, and adherent cells were considered BMMSCs.

2.3. Cell identification

P3 BMMSCs were seeded into T75 flasks (Thermofisher Scientific, Rochester, NY, USA), and media was changed every other day. When the confluence reached ~90%, the cells were harvested and flow cytometry

analysis was performed. The positive rates of cell surface markers CD44-FITC, CD45-FITC, and CD90-PE (Bio Legend, USA) were measured and analyzed.

2.4. Cytotoxicity test

The extracted medium of medical SR tube (Jiangyang Co., Ltd., P.R. China) was prepared with complete culture medium. The extraction ratio was 3 cm^2/mL and extracted on a shaking table at 37 °C for 24 h. P3 BMMSCs were resuspended with fresh medium and incubated at 2 × 104 cells per well in 48-well plates; the liquid per well was 200 μL. On the second day after inoculation, the culture medium was changed for the first time. The Control group was replaced by fresh complete medium, and for the test group it was replaced by the prepared SR extract. On the 1st, 3rd, and 7th day after the first change, six samples from the Control group and test group were taken. Then, 20 μL CCK8 working solution were added and the mixture incubated in the dark for 1 h. The OD value at 450 nm was measured by microplate reader. Relative increment rate (%) = OD value of test group/OD value of Control group.

2.5. Hemolysis test

The extracted normal saline of medical SR tube (Jiangyang Co., Ltd., P.R. China) was prepared with normal saline. The extraction ratio was 3 cm^2/mL and extracted on a shaking table at 37 °C for 24 h. Fresh anticoagulant rabbit blood was used for detection; rabbit blood was diluted to 2%. There were three experimental groups: the positive control was dissolved with triple distilled water, the negative control was dissolved with normal saline, and the test was dissolved with extracted normal saline. diluted rabbit blood (4 mL) was taken from each group, incubated in 37 °C cell incubator for 60 min, and then centrifuged at 2000 rpm for 5 min. Then, 100 μL of each sample was added to a 96 well plate. OD value at 545 nm was measured with microplate reader. The average of each group was used to calculate the hemolysis rate (%). An hemolysis rate ≤5% is regarded as meeting the standard.

2.6. SR cell culture plate preparation

Sylgard SR liquid (Dow Corning, USA) and curing agent (Dow Corning, USA) were mixed in a ratio of 10:1; then, the mixture was centrifuged with a centrifuge at 2000 rpm for 10 min. After adding 1 mL of SR liquid per well into the 12-well plate and distributing it evenly at the bottom of the plate, it was placed on a flat table for 2 weeks to solidify. The cell pore plate was soaked in 75% alcohol for 3 days, disinfected and irradiated with ultraviolet light for 24 h.

2.7. Scanning electron microscope scanning

BMMSCs were cultured on the SR surface for 7 days, and samples were extracted and gently washed with DPBS for 3 times. Each sample was fixed with 4% glutaraldehyde at 4 °C for 1 h and gently rinsed with deionized water for 15 min.

The samples were dehydrated by ethanol gradient (10, 30, 50, 70, 90, 95, 100%) and dried overnight. After spraying gold on the sample surface, the morphology of BMMSCs on the surface of SR was observed.

2.8. Fluorescence microscopy

BMMSCs were cultured on the surface of SR for 3 days, and samples were extracted and gently washed with DPBS for 3 times. BMMSCs were fixed with 4% paraformaldehyde at room temperature for 30 min, and washed with DPBS 3 times. The cells were soaked in 0.1% TritonX-100 (Beyotime Biotechnology, Ltd., P.R. China) for 10 min, and washed with DPBS (Solarbio, Ltd., P.R. China) 3 times. BMMSCs were soaked in 500 μl of TRITC Phalloidin (100 Nm, Solarbio, Ltd., P.R. China), incubated in the dark at 37 °C for 1 h, washed with DPBS 3 times, and soaked in 500 μl DAPI (5 μg/mL, Solarbio, Ltd., P.R. China), incubated in the dark at 37 °C for 5 min, and washed with DPBS 3 times. Finally, BMMSCs were observed and photographed under a fluorescence microscope.

2.9. Live/dead cell staining

BMMSCs were cultured on the surface of SR for 3 days, and stained according to the live/dead cell staining kit instructions (Solarbio, Ltd., P.R. China). BMMSCs were stained in the suspended and adherent states, respectively; then, cells were observed and photographed under a fluorescence microscope. Six visual fields of suspended cells were counted and analyzed with Image J software to calculate the number of live/dead cells.

2.10. Test of BMMSCs' mineralization ability on the SR surface

The osteogenic induction medium had DMEM medium with high glucose (Gibco, Rockville, MD, USA), with 10% fetal bovine serum (FBS, Biological Industries, Israel), 0.01 μmol/L dexamethasone (Sigma–Aldrich, USA), 50 μg/mL β sodium glycerate (Sigma–Aldrich, USA) and 10 mmol/L ascorbic acid (Sigma–Aldrich, USA). BMMSCs were cultured on the SR surface, and after 48 h, in the test group the medium was replaced by osteogenic induction medium, while the Control group continued to use complete medium. After 21 days of continuous culture, the culture medium was discarded and cells were washed by DPBS 3 times. The cells were fixed by 4% paraformaldehyde at 4 °C for 30 min, and stained with 1 mL Alizarin red (1%, pH 4.2, Solarbio, Ltd., P.R. China) per well for 5 min. Finally, the cells were gently washed with double distilled water 3 times, observed and photographed under an inverted phase contrast microscope.

2.11. Bone defect model

Six-month-old New Zealand white rabbits weighing 2.5–3 kg were used in this experiment. An F16 SR tube (outer diameter 5.33 mm, inner diameter 3.33 mm, length 2 cm, Jiangyang, Ltd., P.R. China) was used. Food and water were forbidden 8 h before surgery, weight was weighed, and 2% Cerazine hydrochloride (Huamu, Ltd., P.R. China) was injected intramuscularly at 0.1 mL/kg as anesthesia. A 1.5 cm bone defect was amputated in the middle of the rabbit radius during surgery. The experimental animals were divided into three groups:

① Control group: no other treatment after osteotomy; ② Silicone rubber sealed channel group (SR group): the two ends of the bone defect were sleeved with a 2 cm SR sealed channel; ③ Silicone rubber channel with holes group (SR + Holes group): a 2 cm SR tube was used to connect both ends of bone defect, with one 0.5 × 0.5 cm square hole above and below the SR tube. In the first 3 days after surgery, the wound dressing was changed and 30,000 UI/kg penicillin (Keda, Ltd., P.R. China) was injected. 6 rabbits were sacrificed at eight time points (1, 3, 7.14 days, 4 weeks, 8, 12, and 16 weeks) in each group. The number of animals in the entire experiment was 144. The SR channels were removed in the 12 and 16 weeks groups when at 10 week. The Control group underwent sham surgery.

2.12. ELISA

At four time points (1, 3, 7, and 14 days after surgery), six rabbits in all groups were sacrificed. The SR channel was carefully removed, and the new tissue in the tube extracted. For animals without new tissue, the same volume of soft tissue around the radius was taken. Twenty milligrams of tissue were weighed on an electronic balance and 200 μL normal saline was used to obtain a tissue homogenate, centrifuged at 3000 rpm for 10 min, and the supernatant was tested for osteocalcin (OCN), bone morphogenetic protein-2 (BMP-2), runt-related transcription factor 2 (Runx2), transforming growth factor-β1 (TGF- β1), and VEGF according to the instructions of ELISA kit (Xinquan, Ltd., P.R. China) and the OD

value of each hole measured at 450 nm. Finally, a standard curve was drawn and the concentration of the target protein in each sample calculated.

2.13. X-ray and micro CT

At 4, 8, 12, and 16 weeks after surgery, 6 rabbits in each group were sacrificed, and the ulna and radius of rabbits were excised for X-ray and micro CT examination. The radiographic results of X-ray in each group were evaluated by the Lane-Sandhu score and the 2D CT images were analyzed using CTAn software (SkyScan), which were then evaluated to calculate the percentage of new bone volume relative to tissue volume (BV/TV), trabecular number (Tb. N) and trabecular thickness (Tb. Th).

3.14. Fluorescent labeling of bone tissue

Three rabbits in each group at 16 weeks were injected with fluorescent markers, Alizarin red S at 6 weeks (30 mg/kg, Sigma–Aldrich, USA), tetracycline hydrochloride at 9 weeks (25 mg/kg, Sigma–Aldrich, USA) and calcein at 12 weeks (25 mg/kg, Sigma–Aldrich, USA). The specimens were cut into hard tissue sections for observation by laser confocal microscope.

2.15. Masson and safranine O staining

Specimens all groups were fixed with 4% paraformaldehyde for 48 h. After decalcification with EDTA decalcification solution, paraffin sections were stained with Masson staining kit (Solarbio, Ltd., P.R. China) and modified safranin O staining kit (Solarbio, Ltd., P.R. China).

2.16. CD31 immunohistochemical staining

Specimens in all groups were fixed with 4% paraformaldehyde for 48 h. After decalcification with EDTA decalcification solution, CD31 (Abcam, UK, Antibody concentration was 1:100) immunohistochemical staining was performed on the specimens. The CD31 positive area was calculated by Image J.

2.17. Statistics

The experimental results were analyzed by SPSS13 0 software for data analysis. All data are expressed as mean ± standard deviation. The threshold for statistical significance was set at $P < 0.05$.

3. Results

3.1. BMMSC extraction and identification

BMMSCs were isolated from SD rats and cultured in vitro. P3 BMMSCs grew in spindle shape under the microscope. The expression of surface markers (CD 34, CD 44, CD 45 and CD 90) in P3 BMMSCs was detected by flow cytometry. The results showed: 99.9% expression positive rate of BMMSCs positive marker CD 44, 99.9% (>95%) positive CD 90 expression rate; 4.43% expression of negative CD 34 marker, and 0.81% (<5%) CD 45 expression (Supplementary information 1).

3.2. Cytotoxicity and hemolysis tests

The OD value measured by CCK 8 method on the first, third, and seventh days. The relative proliferation rates of BMMSCs cultured with SR extract were 92.0%, 82.5% and 97.6% on day 1, day 3, and day 7, respectively. The cytotoxicity grade was grade I, which met the toxicity requirements of implant materials. The hemolysis test showed hemolysis in the positive Control group. The OD value at 545 nm is shown in Table 1. The hemolysis rate of the experimental group was 0.20% (<5%), indicating that the silicone rubber does not cause hemolysis.

Table 1
Hemolysis test results.

Groups	OD value						OD value (Mean ± SD)
	1	2	3	4	5	6	
Negative control	0.010	0.010	0.012	0.012	0.012	0.011	0.011 ± 0.001
Positive control	1.004	1.031	1.020	1.052	1.011	1.047	1.028 ± 0.019
Test group	0.014	0.013	0.013	0.015	0.013	0.012	0.013 ± 0.001

3.3. BMMSC adhesion on the SR surface

An SR cell plate was shown inSupplementary information 1C. After 2 weeks of solidification and shaping period, the SR was a transparent round sheet solid. After aseptic treatment, it could be used for cell inoculation. P3 BMMSCs were inoculated on its surface for 48 h. In an inverted phase contrast microscope, the cells were found to adhere well on the surface of SR, and there were no obvious floating cells or toxic particles in the cells (Supplementary information 1).

Cell morphology of cells cultured on the surface of SR for 7 days on scanning electron microscope (Supplementary information 1). BMMSCs adhere well on the surface of SR and cells fuse with each other in the growth concentration part and cover the surface of SR in a sheet. BMMSCs showed a TRITC Phalloidin labeled cytoskeleton (red) and DAPI labeled nuclear morphology (blue) under fluorescence microscope.Supplementary information 1I–K showed that BMMSCs could adhere and grow in good condition on the SR surface.

3.4. Live/dead cell fluorescent staining

BMMSCs adhered well on the surface of SR and stretched into spindle shape after 3 days of culture. Most cells were stained with green fluorescence (living cells), and only a small proportion of red fluorescence (dead cells). Under co-culture with SR material, BMMSCs grew well and cell survival rate was high, thus meeting the conditions of bone induction implant material (Supplementary information 1).

3.5. BMMSCs' mineralization ability on the SR surface

After 21 days of culture and Alizarin red staining, no calcium nodules were found in Control group, showing that SR material did not induce BMMSCs' osteogenic mineralization. In the osteogenic induction group, BMMSCs on the SR surface were induced by osteogenic culture medium for 21 days. After Alizarin red staining, obvious red calcium nodules appeared, indicating that BMMSCs on the surface of SR had good osteogenic differentiation potential, which could be realized under appropriate induction conditions (Supplementary information 1).

3.6. Observation of animal specimens

A model of 1.5 cm defect of the rabbit radius was established (Fig. 1). The radius diameter of rabbits is shown in supplementary information 2, and the number of each group was 48. There was no significant difference in the radius diameter of each group ($P > 0.05$). The length of bone defect was 4.72 times, 4.69 times, and 4.76 times of the average radius diameter in Control group, SR group, and SR + Holes group, respectively.

In the SR group, hematoma tissue was generated in the SR sealed channel 1 day after surgery, and the hematoma tissue was completely filled in the SR sealed channel (Fig. 2). Carefully dissecting the SR sealed channel, the new hematoma observed as a cylinder, bridging at both ends of the bone defect. The color of hematoma tissue was dark red on the first day after surgery. The new hematoma tissue gradually became yellowish brown from the 7th day to the 14th day (Fig. 2). In the Control and SR + Holes groups, there was no hematoma formation at 1, 3, 7, or 14 days

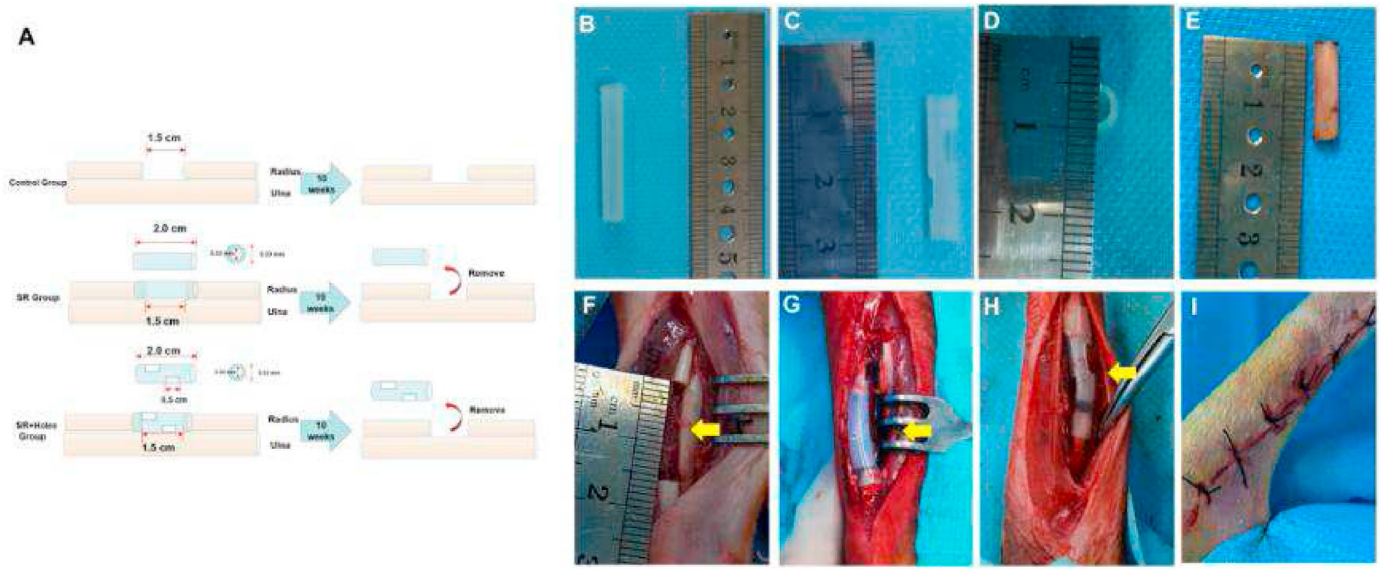

Figure 1. (A) Establishment of a rabbit model of large radial bone defect
(B) Sealed SR channel used in the SR group
(C) SR channel used in the SR + Holes group with two 5 mm × 5 mm square defect holes in the tube wall
(D) SR channel (5.33 mm outer diameter and 3.33 mm inner diameter)
(E) Radial defect during surgery
(F) Control group with 1.5 cm bone defect (shown by yellow arrow)
(G) SR group with 1.5 cm bone defect and an implanted medical SR airtight channel on the defect (shown by yellow arrow)
(H) SR + Holes group with 1.5 cm bone defect and implanted SR channel with holes over the defect (marked with yellow arrow)
(I) Rabbit limb incision sutured layer by layer.

after surgery (Fig. 2). This experiment showed that a SR sealed channel could induce hematoma tissue formation and hematoma could form a bridge at the broken ends of the fracture at an early stage. The SR + Holes group did not form hematoma tissue, indicating that this induction method depends on the complete and sealed environment of the SR channel.

The SR channel was removed at the 10th week after surgery. During surgery, new bone was observed in the SR sealed channel in the SR group, with obvious extension of the fracture end. The fracture end of the bone defect was bridged, and only a few millimeters without ossification remained (Fig. 3). In the SR + Holes group, there was no obvious extension of fracture end, and proliferative fibrous tissue grew into the SR hole leading to bone non-union (Fig. 3). The Control group underwent sham surgery at 10 weeks, in those animals, fibrous scar tissue hyperplasia wrapped the fracture end and bone non-union formed (Fig. 3).

At the 16th week after surgery, the bone defect in SR group was healed, the new bone was completely bridged, and the bone tissue was in good shape (Fig. 3). Fibrous scar tissue hyperplasia and ingrowth and bone non-union was observed at the bone defect in the SR + Holes group (Fig. 3). At 16 weeks, in the Control group, bone non-union was formed at the fracture end, the medullary cavity was closed, and bone resorption occurred (Fig. 3). These results show that the SR sealed channel had a good inductive repair effect on bone defects and that closure of the SR channel is important for bone healing. The occurrence of bone non-union is closely related to the proliferation and growth of fibrous tissue. The SR sealed channel can block the growth of fibrous tissue and provides an appropriate closed environment for bone regeneration.

3.7. ELISA

OCN, BMP-2, TGF-β1, Runx2, and VEGF expression were analyzed quantitatively through ELISA (Fig. 4A). TGF-β1 expression in the SR group on the first (56.53 ± 0.82 pg/mL) and third day (55.73 ± 0.64 pg/mL) after surgery was significantly higher than in the Control and SR + Holes groups ($P < 0.05$). In contrast, TGF-β1 expression did not significantly decrease compared to the Control and SR + Holes groups ($P > 0.05$) at seven days (46.50 ± 1.08 pg/mL), but was significantly lower than the Control and SR + Holes groups ($P < 0.05$) on the 14th day (40.41 ± 1.58 pg/mL). Runx2 expression in the SR group was significantly higher than that in the Control and SR + Holes groups at all timepoints ($P < 0.05$). OCN, BMP-2, and VEGF expression in the SR group was significantly higher than in Control and SR + Holes groups ($P < 0.05$).

There was no significant difference in Runx2, BMP-2, TGF-β1, and VEGF expression between Control and SR + Holes groups at any timepoints ($P > 0.05$).

3.8. X-ray and micro CT

The results of X-ray (Fig. 4B) and Micro CT (Fig. 4D) showed initial extension of the fracture end in animals in the SR group at the 8th week after surgery, bone connection at the 12th week, and bone healing in all animals at the 16th week. At 4, 8, 12, and 16 weeks after surgery, no bone healing was found in the bone defects of any animals in the Control group. At 8 weeks after surgery, the fracture end showed medullary cavity closure; bone non-union and bone resorption occurred at 12 and 16 weeks after surgery. In the SR + Holes group, bone healing was not achieved at 4, 8, 12, or 16 weeks after surgery. From 8 weeks after surgery, there was a partial extension of bone tissue in the porous SR channel, but the final outcome was bone non-union. In the Control group, there was no new bone formation at 4 weeks after surgery, bone non-union and medullary cavity closure initially appeared at 8 weeks after surgery, while bone non-union formed at 12 and 16 weeks after surgery. In the SR + Holes group, there was no bone healing either at 4, 8, 12, and 16 weeks after surgery, and hyperplasia of local fibrous scar tissue formed at 12 and 16 weeks after surgery.

The Lane-Sandhu scores (Fig. 4C) of the SR group were significantly higher than those of the other two groups at 4, 8, 12, and 16 weeks after surgery ($P < 0.05$). At 16 weeks, all specimens had completed bone healing, and some had completed the shaping of medullary cavity and

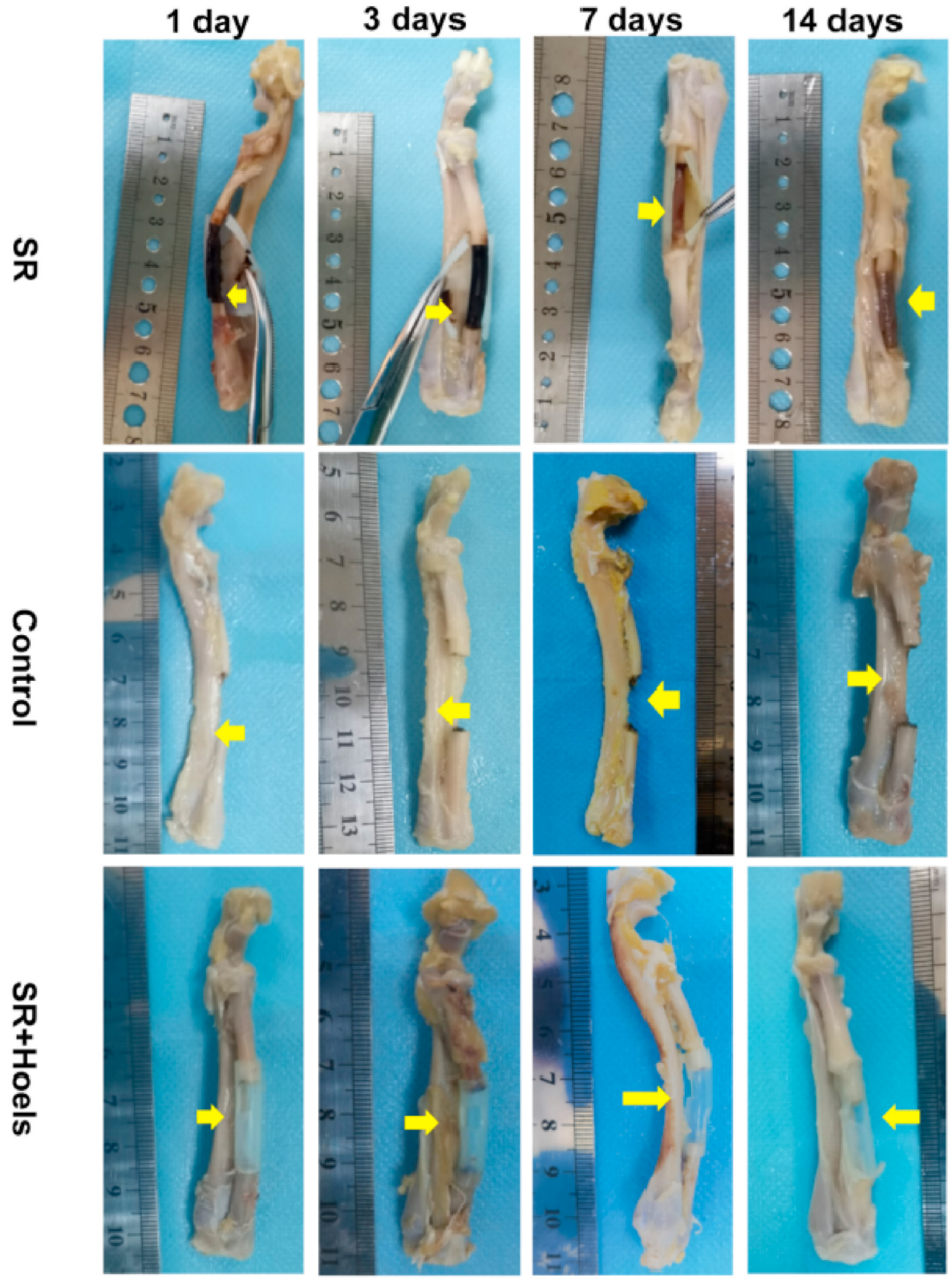

Figure 2. The external images of specimens. Hematoma tissue formed in SR group and no hematoma tissue formed in Control group and SR + Holes group (yellow arrows).

cortical bone. At 12 and 16 weeks, the score of the SR + Holes group was slightly higher than that of the Control group ($P < 0.05$), indicating that the SR channel with holes slightly promoted regeneration of the bone defect. However, due to incomplete closure of the SR channel and proliferation and growth of fibrous tissue, the final outcome was non-union.

The lower threshold used by Micro CT was 80, and the upper threshold was 140 in this in this research. There was no significant difference in the volume of new bone tissue between the SR + Holes and Control groups at 4 weeks (see Fig. 4E). At the 8th week after surgery, the volume of new bone in the SR + Holes group was significantly higher

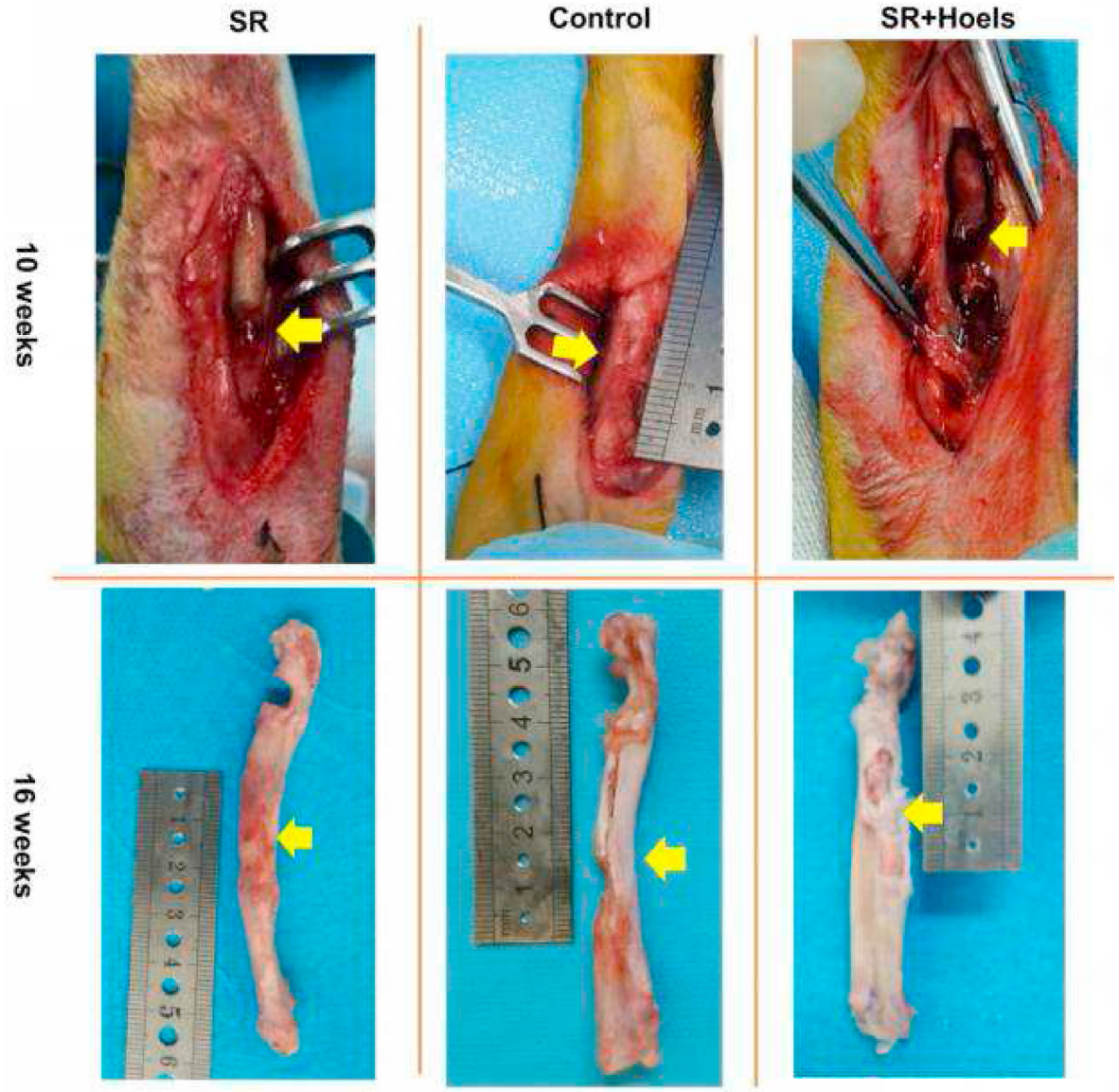

Figure 3. In SR group at 10 weeks, the silastic closed channel was taken out, and the fracture end was obviously extended, with only a few millimeters of space not ossified (yellow arrow). In SR + Holes group at 10 weeks, the silastic channel with holes was taken out, and no bone healing and local fibrous tissue hyperplasia (yellow arrow) were found; fibrous scar tissue hyperplasia (yellow arrow). Control group at 10 weeks, the formation of nonunion, the broken end of the pulp cavity closed (yellow arrow).
SR group at 16 weeks, bone healing was completely achieved (yellow arrow).
SR + Holes group and Control group at 16 weeks, the formation of nonunion, the fibrous tissue growth was obvious (yellow arrows).

than in the Control group ($P = 0.002$), and the volume of new bone in SR group was significantly higher than that in Control group ($P < 0.0001$). At 12 and 16 weeks after surgery, the volume fraction of new bone in SR group reached 43.92 ± 1.74% and 72.22 ± 0.60%, respectively; which was significantly higher than in the other two groups ($P < 0.05$). The volume fraction of new bone in the SR + Holes group was also significantly higher than in the Control group at 12 and 16 weeks ($P < 0.05$). The same trend could also be observed for Tb. N and Tb. Th.

3.9. Fluorescence bone labeling

In the SR group, there was no new bone at the radial defect 6 weeks after surgery; only the morphology of the ulna could be observed, indicating no obvious ossification at the fracture end (Fig. 5). At 9 weeks after surgery, new bone appeared at the radial defect; the middle of the bone defect had been bridged. At the 12th week after surgery, the end of the bone defect was completely bridged, and the defect filled with new bone (Fig. 5). In the Control group, there was no obvious extension of fracture end at 6, 9, and 12 weeks after surgery; the bone defect was non-union (Fig. 5). At 6 weeks, the fracture end in the SR + Holes group showed a little extension compared with the Control group, but there was no difference in bone tissue fluorescence at 6, 9, and 12 weeks after surgery, indicating that the bone defect did not form bone during this period; thus, the fracture end did not achieve bone bridging at 12 weeks (Fig. 5). This experiment confirmed that a large bone defect of rabbit radius induces osteogenesis process of gradual extension and ossification from the broken end of the bone defect to its center.

3.10. Masson staining

In the SR group, hematoma tissue formed in SR sealed channel. Masson staining showed that on the first day after surgery, the new

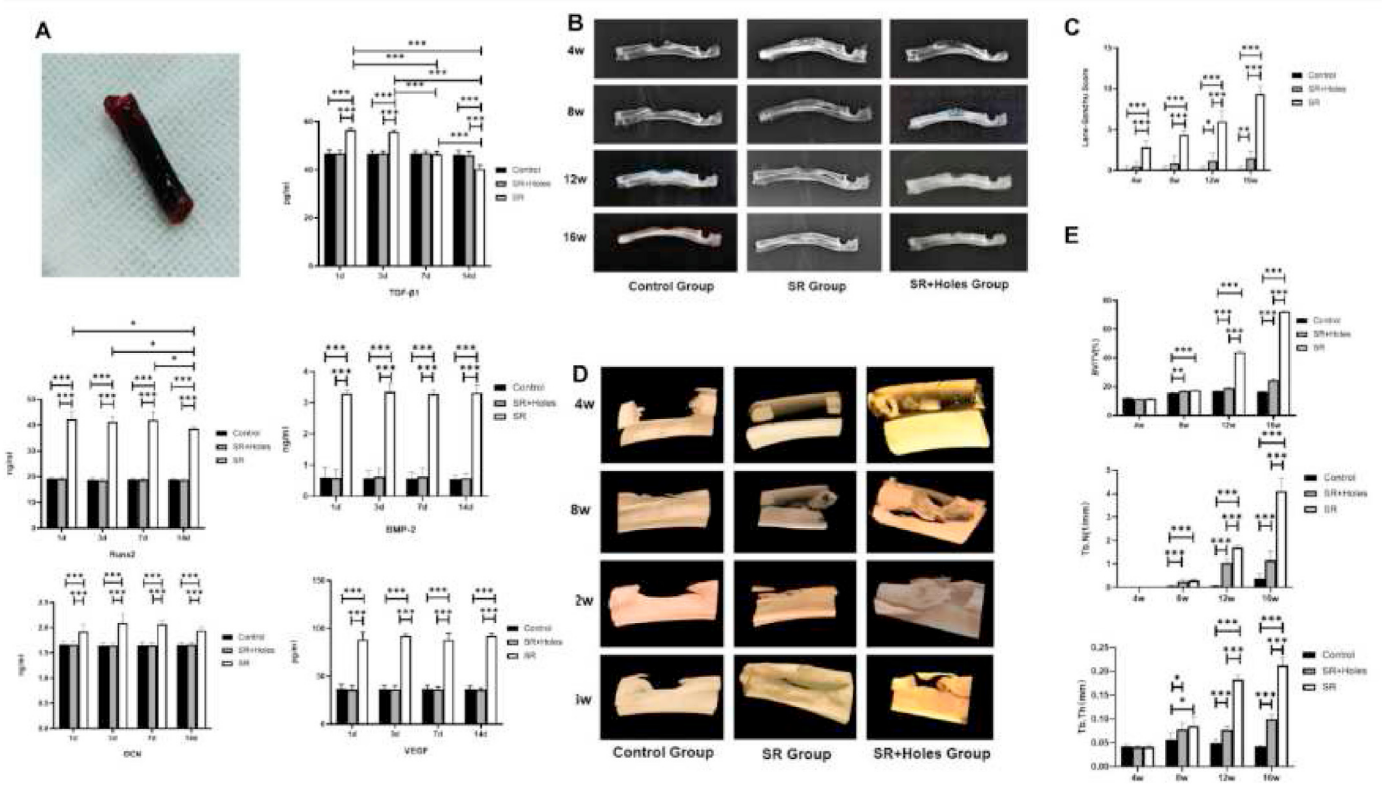

Figure 4. (A) Hematoma tissue and ELISA results of tissue homogenates.
*: $p < 0.05$; **: $p < 0.01$; ***: $p < 0.001$
(B) X-ray results
(C) Lane-Sandhu scoring results.
* : $p < 0.05$; ** : $p < 0.01$; *** : $p < 0.001$
(D) Micro CT results
(E) BV/TV, Tb. N and Tb. Th results.
* : $p < 0.05$; ** : $p < 0.01$; *** : $p < 0.001$.

hematoma tissue was mainly composed of red blood cells (Fig. 6). On the third postoperative day, new capillaries appeared in the hematoma tissue (Fig. 6). On the 7th day, the hematoma tissue showed obvious shrinkage, internal neovascularization continued to increase, and the hematoma began to organize (Fig. 6). On the 14th day, cartilage cells were observed at both ends of the hematoma, and local staining in green (Fig. 6). At 4 weeks, the broken end of the bone defect was filled and bridged by neohematoma tissue, which had obvious branch-like vascular network formation (Fig. 6). At 8 weeks, trabecular bone structures appeared, stained in green (Fig. 6). At 12 weeks, the new tissue was stained red-green, indicating gradually maturing new bone (Fig. 6). At 16 weeks, the red tissue staining continued to increase, only part of the blue-green tissue remained, indicating further maturation of new bone tissue, and that ossification was basically completed (Fig. 6). The Masson staining results of the Control group are shown in Fig. 6. At 4 weeks after surgery, the broken end of the bone defect is stained green, indicating a small amount of new bone reaction at the broken end of the defect, but no extension of the fracture end; the middle part of the bone defect is not bridging. At 8 weeks postoperatively, the stump was still stained green, and hyperplastic fibrous scar tissue starting to wrap the fracture stump. At 12 weeks, the stump of the bone defect was stained red, the medullary cavity closed, and proliferating fibrous scar tissue completely surrounded the stump. At 16 weeks, the results were similar. The results of the SR + Holes group were similar to those of the Control group. At 4 weeks after surgery, no bridging at the broken end of the bone defect was observed. At 8 weeks, fibrous scar tissue and muscle fibers began to appear at the broken end of the fracture. Non-union was formed at 12 and 16 weeks, and the medullary cavity of the broken end was closed (Fig. 6).

3.11. Safranine O staining

Safranine O staining on the 1st and 3rd postoperative days, showed no chondrocytes in the hematoma tissue of the SR group. On the 7th day after surgery, the eosinophilic characteristics of hematoma tissue gradually became neutral at both ends. On the 14th day, the two ends of hematoma tissue showed initial chondrosis (Fig. 7). Four weeks after surgery in the SR group, the hematoma tissue was in the stage of endochondral osteogenesis. At 8 weeks after surgery, the cartilaginous tissue matured gradually, and the new tissue gradually acquired a bone trabecular structure. At 12 weeks, the cartilaginous tissue gradually decreased and the trabeculae matured further. Cartilaginous tissue disappeared almost completely at 16 weeks. This suggests that hematoma ossification is an endochondral osteogenic process. The results of safranine O staining in the Control group are in Fig. 7. At 4 weeks after surgery, no chondrogenic tissue appeared at the broken end of the bone defect. At 8 weeks, the broken end had no cartilaginous tissue and was surrounded by fibrous scar tissue. At 12 weeks, some chondrogenic tissue appeared inside the medullary cavity, tending to seal it, probably because the broken end of the bone defect was surrounded and sealed by fibrous scar tissue. After 16 weeks, the cartilaginous tissue at the end of the bone defect disappeared, the medullary cavity was closed, and the broken end was completely wrapped by fibrous scar tissue. The staining results of safranine O in SR + Holes group can be observed in Fig. 7; no obvious chondrogenization was observed at any each stage. During the process of osteogenesis induced by silastic closed channels, the peak of chondrogenization occurred from the 4th–8th week, and the cartilaginous tissue gradually decreased after 12 weeks, accompanied by mature bone

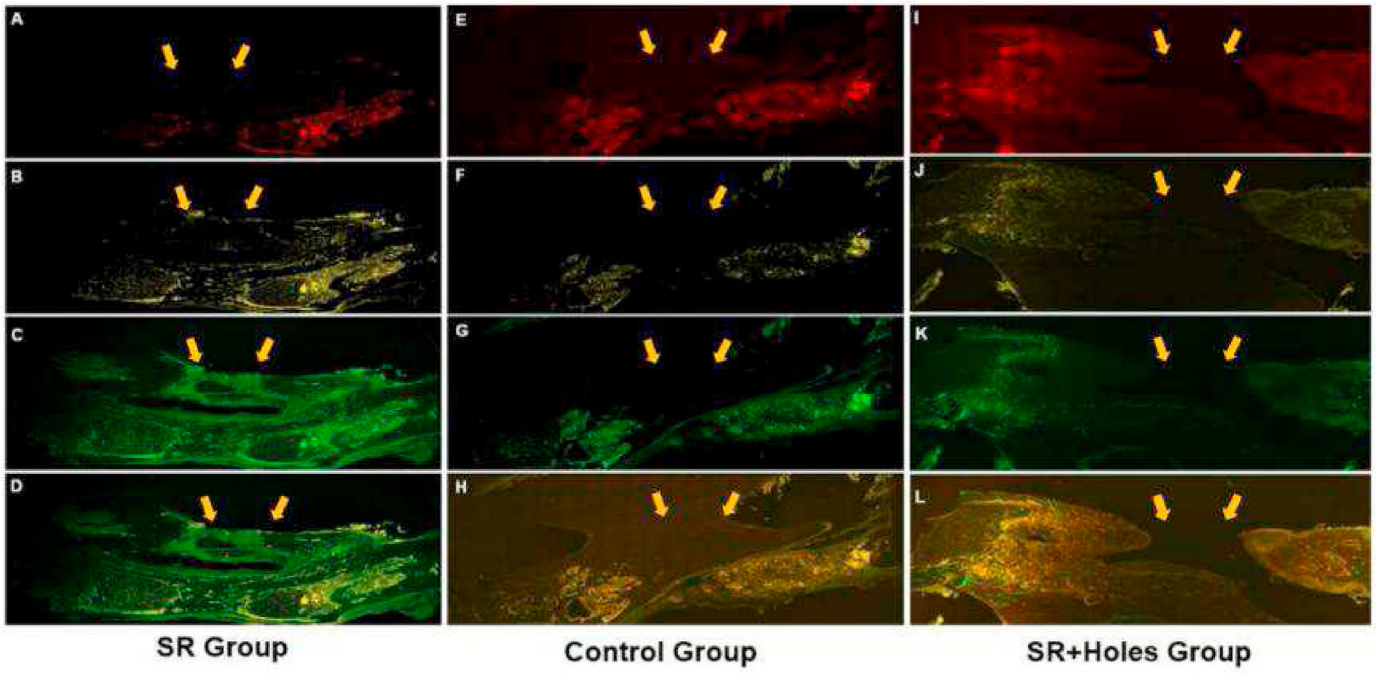

Figure 5. Fluorescent staining of bone tissue
(A) Alizarin red staining showed that there was no new bone in the defect area at 6 weeks in SR group (yellow arrows)
(B) Tetracycline hydrochloride staining showed that new bone formed in the defect area at 9 weeks in SR group (yellow arrows)
(C) Calcein staining showed that the new bone was completed bridging in the defect area at 12 weeks in SR group (yellow arrows)
(D) Fig. A, B, C merged
(E) Alizarin red staining showed that there was no new bone in the defect area at 6 weeks in Control group (yellow arrows)
(F) Tetracycline hydrochloride staining showed that there was no new bone in the defect area at 9 weeks in Control group (yellow arrows)
(G) Calcein staining showed that there was no new bone in the defect area at 12 weeks in Control group (yellow arrows)
(H)Fig. E, F, G merged
(I) Alizarin red staining showed that there was no new bone in the defect area at 6 weeks in SR + Holes group (yellow arrows)
(J) Tetracycline hydrochloride staining showed that there was no new bone in the defect area at 9 weeks in SR + Holes group (yellow arrows)
(K) Calcein staining showed that there was no new bone in the defect area at 12 weeks in SR + Holes group (yellow arrows)
(L) Fig. I, J, Kmerged.

tissue replacement. This process was not achieved in the Control and SR + Holes groups. In this experiment, an important role of the sealed channel is to block the growth of surrounding fibrous tissue, induce forward endochondral osteogenesis, and avoid local medullary cavity sealing.

3.12. CD31 immunohistochemical staining results

In the SR group, no obvious yellowish brown positive cells were found in the hematoma tissue on the first postoperative day (Fig. 8). On the 3rd postoperative day, CD31-positive cells appeared in the hematoma tissue; connections were dendritic, and the course mostly perpendicular to the longitudinal axis of the new hematoma tissue. On the 7th day after surgery, a thick tubular structure appeared over CD31 positive vessels in the hematoma tissue, and strong CD31 expression was observed at the edge of the hematoma tissue, showing strong vascularization was at the edge of the hematoma tissue. On the 14th day after surgery, a lamellar vascular network appeared on the edge of the hematoma tissue, with growing blood vessels inside. The hematomas were more densely packed at the edge of the tissue and wrapped in a fine mesh throughout the outermost layer of hematoma tissue (Fig. 8). The number of CD31 positive vessels significantly increased ($p < 0.05$) and the blood supply in hematoma gradually increased after surgery (Fig. 8E).

Later, at 4 weeks, the fracture end was bridged by hematoma tissue; there was positive CD31 expression, indicating abundant blood supply and neovascularization inside the hematoma tissue. At 8 weeks, ossification of the new bone tissue was initially observed, and CD31 expression was found in the internal trabecular structure. The new blood vessels were distributed in the whole new bone tissue, showing a fine reticular structure, which confirmed that the osteogenesis process in the new bone tissue was accompanied by vascularization. Abundant CD31 expression was observed in the new bone at 12 and 16 weeks postoperatively. In Control and SR + Holes groups, because bridging was not achieved, we observed the periphery of the fracture end. In the Control group, it was mainly hyperplastic fibrous scar tissue, and there was little CD31 expression. In the SR + Holes group, little CD31 positive tissue was observed at the broken end 8 weeks after surgery (Fig. 8). The fracture end was gradually occluded by connective tissue in later stages, and the medullary cavity of the fracture end was closed at 12 and 16 weeks after surgery, without formation of new bone with good blood supply. The quantitative CD31 results in long-term induced specimens are shown in Fig. 8G. At 4, 8, 12, and 16 weeks, the area of neovascularization in the SR group was significantly bigger than that in Control and SR + Holes groups ($p < 0.05$), indicating that the silastic sealed channel can significantly promote neovascularization. Neovascularization in the SR + Holes group was also significantly higher than in the Control group ($p < 0.05$), indicating that the porous SR channel also had a certain inductive effect, although significantly lower than that of the closed SR channel due to its inability to block fibrous tissue growth.

4. Discussion

Fracture healing is a complex biological process. If bone healing cannot be performed in one-stage, most long tubular bone defects lead to

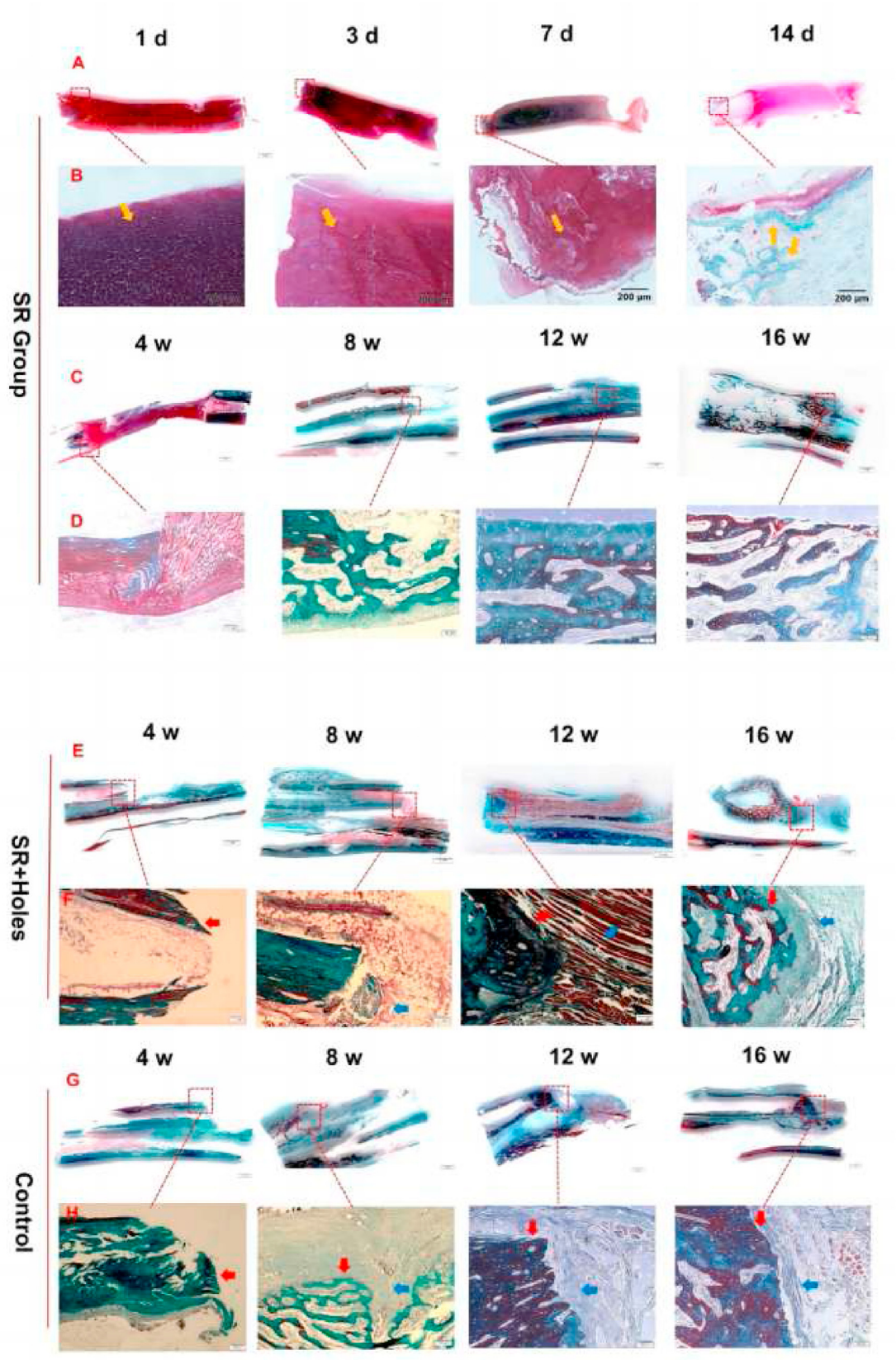

Figure 6. Masson staining results
(A,C,E,D) magnification × 4 (B,D,F,H) magnification × 100
(B) Cartilage cells were observed at both ends of the hematoma at 14 days (shown by blue arrow)
(F,H) The fracture end was shown by red arrows, and fibrous tissue was shown by blue arrow.

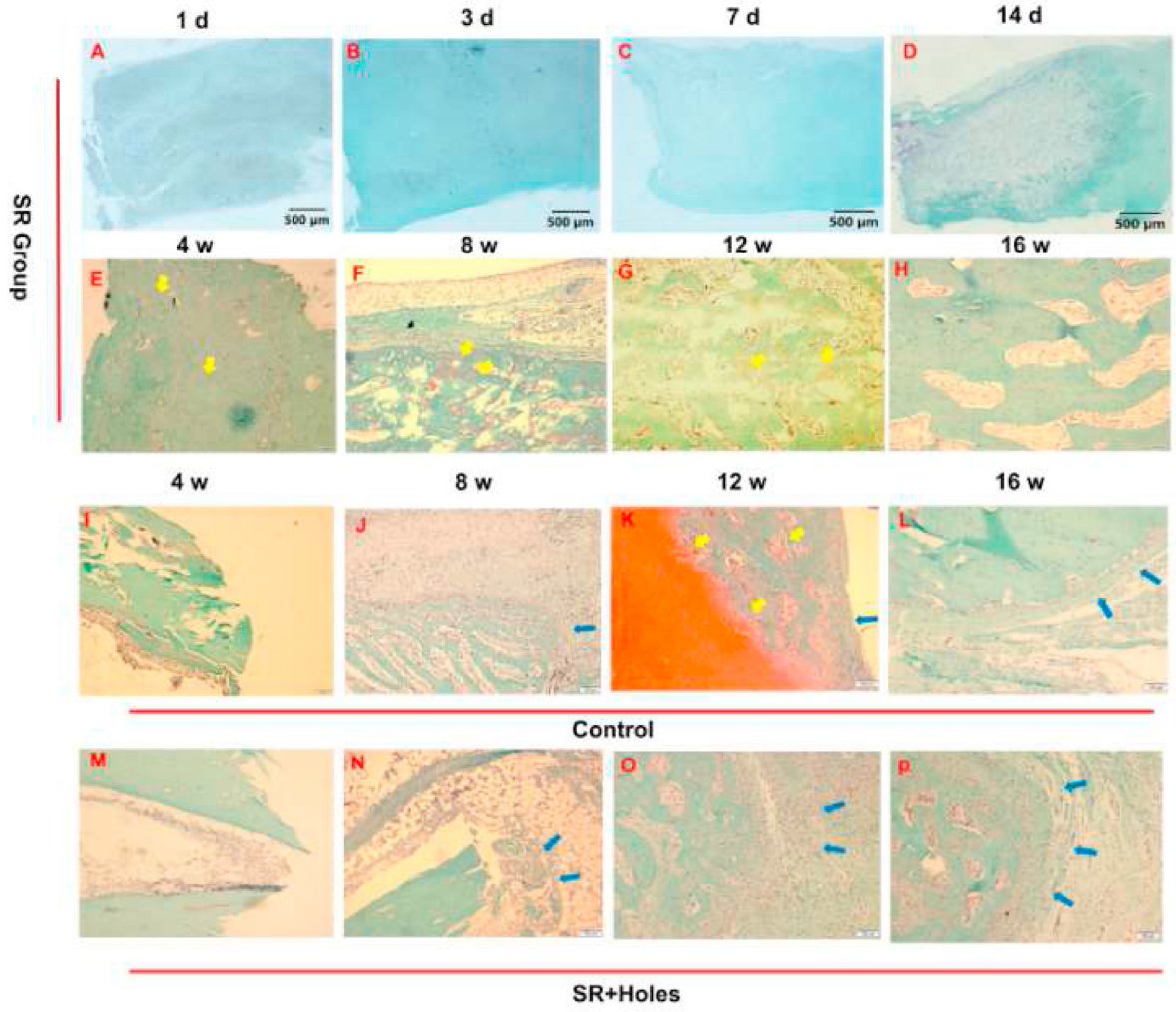

Figure 7. Safranin O staining results (The cartilage is shown by yellow arrows; The proliferative microstructure is shown by a blue arrows) (A–D) magnification × 40 (E–H) magnification × 100.
(I-L) magnification×100; (M-P) magnification×100.

atrophic non-union due to the lack of bone and blood supply. Therefore, the treatment of large defect of long tubular bone should focus on bone healing first stage, to avoid bone non-union, reduce the pain, and improve quality of life and limb function. Fracture healing involves four stages: formation of a blood clot at the site of injury, an inflammatory phase involving specific cell types typical of the innate immune response, callus generation wherein skeletal stem cells are recruited and differentiate into chondrocytes, primary bone formation in which stem cells are recruited to form bone, and secondary bone remodeling involving osteoclasts [77].

In this study, "SR sealed channel induced repair of large defect of long tubular bone" was proposed for the first time. A sealed SR channel was used to connect the two ends of a bone defect. In our experiment, the key factors leading to bone nonunion in the control group are the growth of fibrous tissue and the wrapping of the broken ends of the bone. SR sealed channel created a sealed environment and prevented the fibrous tissue from entering the bone defect, effectively avoiding bone non-union. Although previous studies suggested that spontaneous healing could usually be expected with conventional fixation techniques when the defect was less than 2 cm or involving no more than 50% circumference of the bone [78]. However, our experimental results confirmed that when soft tissue did not become ingrained and ingrowth, under certain conditions, the limit of self-healing might be greater than we expected. The experimental results showed that the SR material could not directly induce BMMSCs' osteogenesis and mineralization, further showing that the key factor for osteogenesis was the sealed environment provided by the channel. Compared with the Masquelet technique, the main advantage of the present method is that it does not require bone grafting, nor did it require seed cells and complex synthetic materials, like tissue engineering. It is a new method of bone induction and a new concept of osteogenesis. In this study, the defect length was >4.5 times the bone diameter. The results reveal that "SR sealed channel induced repair of large defects of long tubular bones" led to endochondral osteogenesis. Hematoma tissue was formed in the sealed channel in the early stage, and bridging was formed at both ends of the bone defect. The hematoma tissue was rich in osteogenesis-related proteins, angiogenesis related protein, and TGF-β1, which could effectively induce osteogenesis. This induction method depended on the sealed environment of SR channel. Our experiments confirmed that the SR material has good biocompatibility and meets the implantation standards of osteoinductive materials and that the SR material does not induce direct osteogenic mineralization of BMMSCs, although they maintain their osteogenic mineralization ability on the SR surface, and can achieve osteogenic mineralization under appropriate conditions. We reviewed the process of SR closed channel induced repair of large bone defects in rabbit's long canal bone (Fig. 9). After surgical implantation of a silastic closed channel, hematoma tissue began to form in the silastic channel 1 day after surgery, with secretion of inflammatory factors and osteogenic and vascular related

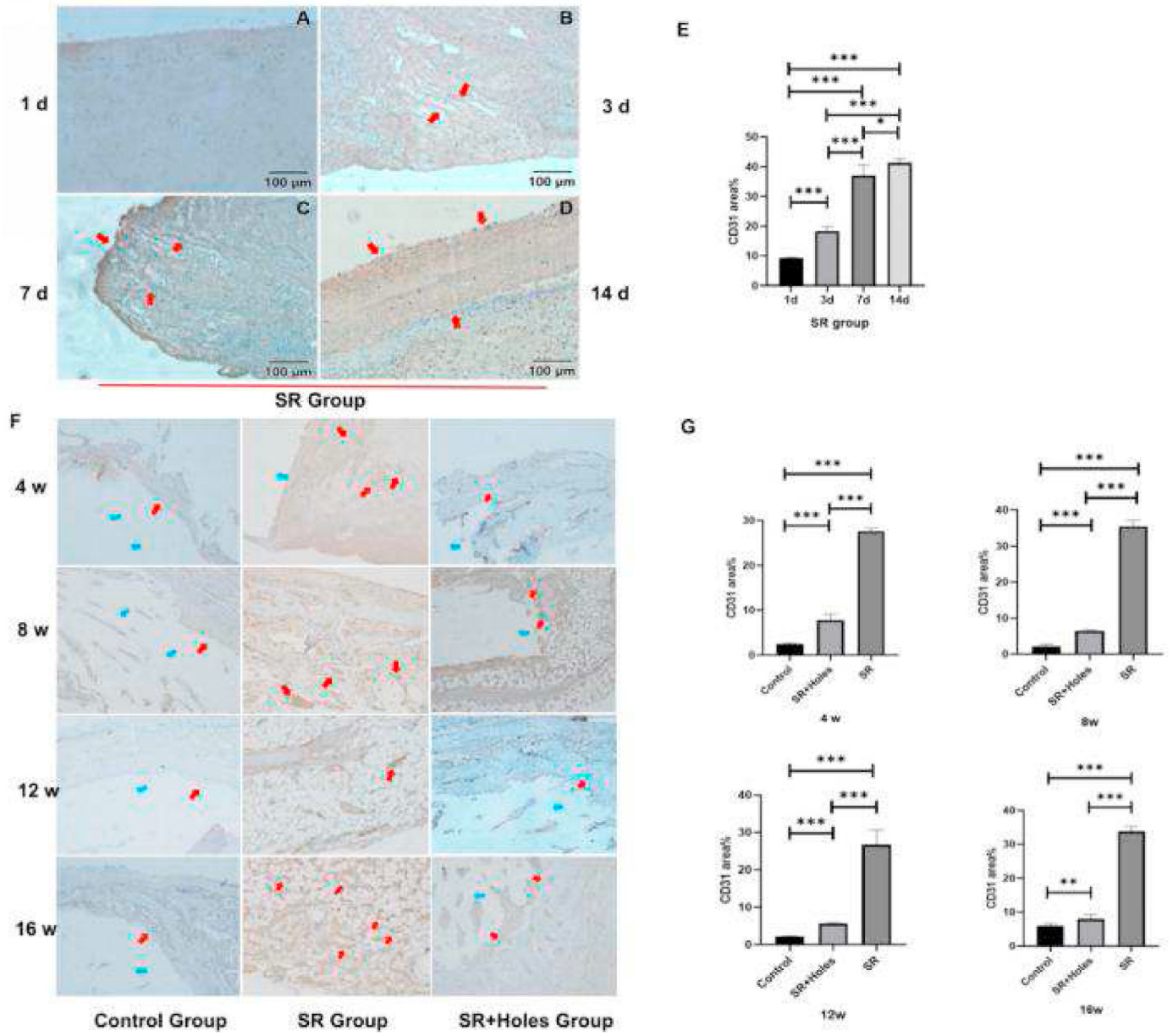

Figure 8. Immunohistochemical staining of CD31
(A) No obvious positive CD31 expression 1 day after surgery in SR Group (× 200)
(B) Positive CD31 expression appeared 3 days after surgery (red arrows) (× 200)
(C) The positive expression of CD31 at 7 days after surgery in SR Group. It was particularly evident at the margins (red arrows) (× 200)
(D) 14 days after surgery, lamellar vascular networks on the margins of the nascent hematoma tissue in a fine mesh wrapped throughout the outer layer of the nascent tissue in SR Group (× 200)
(E) Quantitative CD31 measurements in induced hematoma tissue in the SR group.
*: $p < 0.05$; **: $p < 0.01$; ***; $p < 0.001$
(F) CD31 staining results at 4, 8, 12 and 16 weeks (CD31 positive cells were marked with red arrows, and fracture ends were marked with blue arrows) (× 100)
(G) Quantitative CD31 immunohistochemical results.
*: $p < 0.05$; **: $p < 0.01$; ***: $p < 0.001$.

factors (OCN, BMP-2, Runx2, TGF-β1 and VEGF). Hematoma tissue in 7 days to 4 weeks, gradually appear obvious vascularization reaction, hematoma inside gradually filled by neovascularization, the formation of blood-rich dendritic network. Between 4 and 8 weeks, the new tissue showed a peak of chondrogenesis and the hematoma entered endochondral osteogenesis. At 10 weeks, we removed the SR channel, and at 16 weeks, bone healing was completed. In this experiment, all the rabbits in SR group achieved complete healing of a 1.5 cm bone defect. We speculated that a 2.0 cm bone defect might also achieve healing, but for longer bone defects, it could still be difficult to heal without bone grafting. Based on previous research, periosteal stem cells played an important role in intramembrane osteogenesis [79–82]. Recent research also proved that periosteal stem cells were necessary in the process of endochondral osteogenesis [79]. In this study, bone healing was endochondral osteogenesis process, and we believed that the stem cells involved in this process came from both bone marrow and periosteum. Since bone grafting was not involved in our study, the recruitment of stem cells became the key to bone healing. Both bone marrow and periosteal stem cells require good soft tissue conditions and blood supply around the fracture site. The bone healing process was difficult to

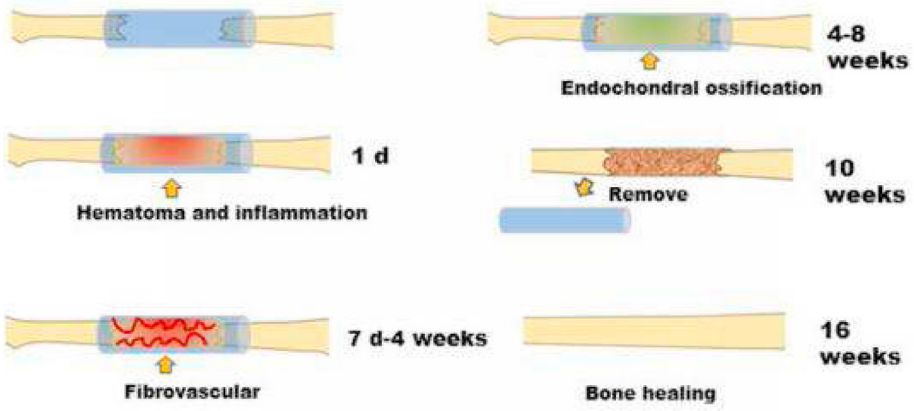

Figure 9. Osteogenesis induced by a silicone rubber sealed channel.

succeed in patients whose soft tissue could not be covered, periosteum was damaged, or blood supply was significantly damaged. In cases with application limitations, we might try using SR sealed channel to shorten the length of bone defects and combine traction osteogenesis technology to achieve bone healing. This part had not been validated yet, and we believed this might be one of the future directions for application.

Previous research has focused on new biomaterials, osteogenic factors, etc [83,84]. However, in our experiments, SR materials did not function in this way. As already mentioned it is not the SR material, but the special environment of the SR sealed channel, that leads to bone healing through endochondral osteogenesis. When the SR tube is incomplete, the hematoma tissue cannot be successfully induced in the tube, resulting in non-union. The first step in fracture healing is hematoma formation, which plays a critical role in fracture [85]. The environment provided by the SR sealed channel allows early hematoma formation, prevents fibrous tissue growth, and finally leads to bone self-healing. According to previous studies, bone tissue contains densely distributed sensory neuronal fibers [86], which are likely to be accompanied by neural network regeneration during the process of bone regeneration, and this process may be related to the regulation of calcitonin gene-related peptide (CGRP). However, further exploration of its specific mechanism is still needed [87,88].

This work proves the effectiveness of an SR sealed channel in inducing repair of large bone defects of long canal bones. Further research is needed to clarify the osteogenic mechanisms involved. SR is a non absorbable material that requires surgical removal. This will cause secondary trauma to patients and also increase their psychological burden, so we believe that the exploration of absorbable materials is necessary. Any non-toxic biomaterial had the potential for application, as long as it could provide a stable and enclosed environment that allowed hematoma formation, but there had been no specific experimental confirmation of this. In further experiments, we believed that SR could be replaced by absorbable materials that did not need to be removed, such as polylactic acid, which is one of our further research directions.

Authors contributions

All authors contributed to the study conception and design. Tiecheng Yu conceived the study, the experiment and manuscript were completed by Feng Gu, and Ke Zhang critically revised the manuscript, Wan-an Zhu, Zhenjiang Sui, Jiangbi Li and Xiaoping Xie performed the literature search and data analysis. All authors read and approved the final manuscript.

Declaration of competing interest

The authors have no conflicts of interest relevant to this article.

Acknowledgments

This study was carried out in accordance with the guidelines for the care for animal subjects adopted by Jilin University; the study protocol was approved by the Research Ethics Committee of the School of Basic Medical Science, Jilin University (ref. no. 2021–125). All SD rats were purchased from Yisi Experimental Technology Co., Ltd., Changchun, P.R. China with animal license No.: SYXK (JI) 2019–0015. All rabbits were purchased from Yisi Experimental Technology Co., Ltd., Changchun, P.R. China with animal license No.: SYXK (JI) 2017–0003.

This study was supported by the National Natural Science Foundation of China (project approval No.31970090) and the Natural Science Foundation of Jilin Province (No. YDZJ202301ZYTS367).

Appendix A. Supplementary data

Supplementary data to this article can be found online at https://doi.org/10.1016/j.jot.2023.09.001.

References

[1] Li Y, Chen SK, Li L, Qin L, Wang XL, Lai YX. Bone defect animal models for testing efficacy of bone substitute biomaterials. J Orthop Translat 2015;3(3):95–104 [eng].
[2] Laubach M, Suresh S, Herath B, Wille ML, Delbrück H, Alabdulrahman H, et al. Clinical translation of a patient-specific scaffold-guided bone regeneration concept in four cases with large long bone defects. J Orthop Translat 2022;34:73–84 [eng].
[3] Schmitz JP, Hollinger JO. The critical size defect as an experimental model for craniomandibulofacial nonunions. Clin Orthop Relat Res 1986;205:299–308 [eng].
[4] Mauffrey C, Barlow BT, Smith W. Management of segmental bone defects. J Am Acad Orthop Surg 2015;23(3):143–53 [eng].
[5] Rimondini L, Nicoli-Aldini N, Fini M, Guzzardella G, Tschon M, Giardino R. In vivo experimental study on bone regeneration in critical bone defects using an injectable biodegradable PLA/PGA copolymer. Oral Surg Oral Med Oral Pathol Oral Radiol Endod 2005;99(2):148–54 [eng].
[6] Ebraheim NA, Elgafy H, Xu R. Bone-graft harvesting from iliac and fibular donor sites: techniques and complications. J Am Acad Orthop Surg 2001;9(3):210–8 [eng].
[7] De Long Jr WG, Einhorn TA, Koval K, McKee M, Smith W, Sanders R, et al. Bone grafts and bone graft substitutes in orthopaedic trauma surgery. A critical analysis. J Bone Joint Surg Am 2007;89(3):649–58 [eng].
[8] Tarng YW, Lin KC. Management of bone defects due to infected non-union or chronic osteomyelitis with autologous non-vascularized free fibular grafts. Injury 2020;51(2):294–300 [eng].
[9] Hertel R, Gerber A, Schlegel U, Cordey J, Rüegsegger P, Rahn BA. Cancellous bone graft for skeletal reconstruction. Muscular versus periosteal bed–preliminary report. Injury 1994;25(Suppl 1):A59–70 [eng].
[10] Weiland AJ, Phillips TW, Randolph MA. Bone grafts: a radiologic, histologic, and biomechanical model comparing autografts, allografts, and free vascularized bone grafts. Plast Reconstr Surg 1984;74(3):368–79 [eng].
[11] Xie K, Wang L, Guo Y, Zhao S, Yang Y, Dong D, et al. Effectiveness and safety of biodegradable Mg-Nd-Zn-Zr alloy screws for the treatment of medial malleolar fractures. J Orthop Translat 2021;27:96–100 [eng].
[12] Pan Q, Li Y, Xu J, Kang Y, Li Y, Wang B, et al. The effects of tubular structure on biomaterial aided bone regeneration in distraction osteogenesis. Journal of Orthopaedic Translation 2020;25:80–6.

[13] Li Y, Pan Q, Xu J, He X, Li HA, Oldridge DA, et al. Overview of methods for enhancing bone regeneration in distraction osteogenesis: potential roles of biometals. J Orthop Translat 2021;27:110–8 [eng].
[14] Britten S, Ghoz A, Duffield B, Giannoudis PV. Ilizarov fixator pin site care: the role of crusts in the prevention of infection. Injury 2013;44(10):1275–8 [eng].
[15] Simpson AH, Halliday J, Hamilton DF, Smith M, Mills K. Limb lengthening and peripheral nerve function-factors associated with deterioration of conduction. Acta Orthop 2013;84(6):579–84 [eng].
[16] Rozis M, Benetos I, Afrati SR, Polyzois VD, Pneumaticos SG. Results and outcomes of combined cross screw and Ilizarov external fixator frame in ankle fusion. J Foot Ankle Surg 2020;59(2):337–42 [eng].
[17] Morasiewicz P, Dejnek M, Orzechowski W, Urbański W, Kulej M, Dragan S, et al. Clinical evaluation of ankle arthrodesis with Ilizarov fixation and internal fixation. BMC Muscoskel Disord 2019;20(1):167 [eng].
[18] Kirienko A, Malagoli E. Ilizarov technique in severe pediatric foot disorders. Foot Ankle Clin 2021;26(4):829–49 [eng].
[19] García-Cimbrelo E, Olsen B, Ruiz-Yagüe M, Fernandez-Baíllo N, Munuera-Martínez L. Ilizarov technique. Results and difficulties. Clin Orthop Relat Res 1992; 283:116–23 [eng].
[20] Luo S, Kong L, Wang J, Nie H, Luan B, Li G. Development of modified Ilizarov hip reconstruction surgery for hip dysfunction treatment in adolescent and young adults. J Orthop Translat 2021;27:90–5 [eng].
[21] Tarchala M, Harvey EJ, Barralet J. Biomaterial-stabilized soft tissue healing for healing of critical-sized bone defects: the masquelet technique. Adv Healthcare Mater 2016;5(6):630–40 [eng].
[22] Careri S, Vitiello R, Oliva MS, Ziranu A, Maccauro G, Perisano C. Masquelet technique and osteomyelitis: innovations and literature review. Eur Rev Med Pharmacol Sci 2019;23(2 Suppl):210–6 [eng].
[23] Alford AI, Nicolaou D, Hake M, McBride-Gagyi S. Masquelet's induced membrane technique: review of current concepts and future directions. J Orthop Res 2021; 39(4):707–18 [eng].
[24] Morelli I, Drago L, George DA, Gallazzi E, Scarponi S, Romanò CL. Masquelet technique: myth or reality? A systematic review and meta-analysis. Injury 2016; 47(Suppl 6):S68–s76 [eng].
[25] Klein C, Monet M, Barbier V, Vanlaeys A, Masquelet AC, Gouron R, et al. The Masquelet technique: current concepts, animal models, and perspectives. J Tissue Eng Regen Med 2020;14(9):1349–59 [eng].
[26] Mühlhäusser J, Winkler J, Babst R, Beeres FJP. Infected tibia defect fractures treated with the Masquelet technique. Medicine (Baltim) 2017;96(20):e6948 [eng].
[27] Koch TG, Berg LC, Betts DH. Current and future regenerative medicine - principles, concepts, and therapeutic use of stem cell therapy and tissue engineering in equine medicine. Can Vet J 2009;50(2):155–65 [eng].
[28] Zhang W, Wang N, Yang M, Sun T, Zhang J, Zhao Y, et al. Periosteum and development of the tissue-engineered periosteum for guided bone regeneration. J Orthop Translat 2022;33:41–54 [eng].
[29] Li B, Wang X, Wang Y, Gou W, Yuan X, Peng J, et al. Past, present, and future of microcarrier-based tissue engineering. J Orthop Translat 2015;3(2):51–7 [eng].
[30] Ai C, Lee YHD, Tan XH, Tan SHS, Hui JHP, Goh JC. Osteochondral tissue engineering: perspectives for clinical application and preclinical development. J Orthop Translat 2021;30:93–102 [eng].
[31] Sun AR, Udduttula A, Li J, Liu Y, Ren PG, Zhang P. Cartilage tissue engineering for obesity-induced osteoarthritis: physiology, challenges, and future prospects. J Orthop Translat 2021;26:3–15 [eng].
[32] Boskey AL, Coleman R. Aging and bone. J Dent Res 2010;89(12):1333–48 [eng].
[33] Pilitsis JG, Lucas DR, Rengachary SS. Bone healing and spinal fusion. Neurosurg Focus 2002;13(6):e1 [eng].
[34] Loi F, Córdova LA, Pajarinen J, Lin TH, Yao Z, Goodman SB. Inflammation, fracture and bone repair. Bone 2016;86:119–30 [eng].
[35] Giannoudis PV, Einhorn TA, Marsh D. Fracture healing: the diamond concept. Injury 2007;38(Suppl 4):S3–6 [eng].
[36] Marsell R, Einhorn TA. The biology of fracture healing. Injury 2011;42(6):551–5 [eng].
[37] Gerstenfeld LC, Alkhiary YM, Krall EA, Nicholls FH, Stapleton SN, Fitch JL, et al. Three-dimensional reconstruction of fracture callus morphogenesis. J Histochem Cytochem 2006;54(11):1215–28 [eng].
[38] Oryan A, Monazzah S, Bigham-Sadegh A. Bone injury and fracture healing biology. Biomed Environ Sci 2015;28(1):57–71 [eng].
[39] Runyan CM, Gabrick KS. Biology of bone formation, fracture healing, and distraction osteogenesis. J Craniofac Surg 2017;28(5):1380–9 [eng].
[40] Ishii M, Sun J, Ting MC, Maxson RE. The development of the calvarial bones and sutures and the pathophysiology of craniosynostosis. Curr Top Dev Biol 2015;115: 131–56 [eng].
[41] Percival CJ, Richtsmeier JT. Angiogenesis and intramembranous osteogenesis. Dev Dynam 2013;242(8):909–22 [eng].
[42] Walters G, Pountos I, Giannoudis PV. The cytokines and micro-environment of fracture haematoma: current evidence. J Tissue Eng Regen Med 2018;12(3): e1662–77 [eng].
[43] Pfeiffenberger M, Bartsch J, Hoff P, Ponomarev I, Barnewitz D, Thöne-Reineke C, et al. Hypoxia and mesenchymal stromal cells as key drivers of initial fracture healing in an equine in vitro fracture hematoma model. PLoS One 2019;14(4): e0214276 [eng].
[44] Shiu HT, Leung PC, Ko CH. The roles of cellular and molecular components of a hematoma at early stage of bone healing. J Tissue Eng Regen Med 2018;12(4): e1911–25 [eng].
[45] Nich C, Takakubo Y, Pajarinen J, Ainola M, Salem A, Sillat T, et al. Macrophages-Key cells in the response to wear debris from joint replacements. J Biomed Mater Res 2013;101(10):3033–45 [eng].
[46] Kolar P, Schmidt-Bleek K, Schell H, Gaber T, Toben D, Schmidmaier G, et al. The early fracture hematoma and its potential role in fracture healing. Tissue Eng Part B 2010;16(4):427–34 [eng].
[47] Gerstenfeld LC, Cullinane DM, Barnes GL, Graves DT, Einhorn TA. Fracture healing as a post-natal developmental process: molecular, spatial, and temporal aspects of its regulation. J Cell Biochem 2003;88(5):873–84 [eng].
[48] Chen X, Hu C, Wang G, Li L, Kong X, Ding Y, et al. Nuclear factor-κB modulates osteogenesis of periodontal ligament stem cells through competition with β-catenin signaling in inflammatory microenvironments. Cell Death Dis 2013;4(2):e510 [eng].
[49] Cao JY, Wang B, Tang TT, Wen Y, Li ZL, Feng ST, et al. Exosomal miR-125b-5p deriving from mesenchymal stem cells promotes tubular repair by suppression of p53 in ischemic acute kidney injury. Theranostics 2021;11(11):5248–66 [eng].
[50] D'Souza N, Burns JS, Grisendi G, Candini O, Veronesi E, Piccinno S, et al. MSC and tumors: homing, differentiation, and secretion influence therapeutic potential. Adv Biochem Eng Biotechnol 2013;130:209–66 [eng].
[51] Ullah M, Liu DD, Thakor AS. Mesenchymal stromal cell homing: mechanisms and strategies for improvement. iScience 2019;15:421–38 [eng].
[52] Owston HE, Moisley KM, Tronci G, Russell SJ, Giannoudis PV, Jones E. Induced periosteum-mimicking membrane with cell barrier and multipotential stromal cell (MSC) homing functionalities. Int J Mol Sci 2020;21(15) [eng].
[53] van der Kraan PM, Blaney Davidson EN, Blom A, van den Berg WB. TGF-beta signaling in chondrocyte terminal differentiation and osteoarthritis: modulation and integration of signaling pathways through receptor-Smads. Osteoarthritis Cartilage 2009;17(12):1539–45 [eng].
[54] Wang W, Rigueur D, Lyons KM. TGFβ signaling in cartilage development and maintenance. Birth Defects Res C Embryo Today 2014;102(1):37–51 [eng].
[55] Tsiridis E, Upadhyay N, Giannoudis P. Molecular aspects of fracture healing: which are the important molecules? Injury 2007;38(Suppl 1):S11–25 [eng].
[56] Luginbuehl V, Meinel L, Merkle HP, Gander B. Localized delivery of growth factors for bone repair. Eur J Pharm Biopharm 2004;58(2):197–208 [eng].
[57] Claes L, Recknagel S, Ignatius A. Fracture healing under healthy and inflammatory conditions. Nat Rev Rheumatol 2012;8(3):133–43 [eng].
[58] Schindeler A, McDonald MM, Bokko P, Little DG. Bone remodeling during fracture repair: the cellular picture. Semin Cell Dev Biol 2008;19(5):459–66 [eng].
[59] Boyce BF, Xing L. Functions of RANKL/RANK/OPG in bone modeling and remodeling. Arch Biochem Biophys 2008;473(2):139–46 [eng].
[60] Kim JM, Lin C, Stavre Z, Greenblatt MB, Shim JH. Osteoblast-Osteoclast communication and bone homeostasis. Cells 2020;9(9) [eng].
[61] Chen X, Wang Z, Duan N, Zhu G, Schwarz EM, Xie C. Osteoblast-osteoclast interactions. Connect Tissue Res 2018;59(2):99–107 [eng].
[62] Park-Min KH. Metabolic reprogramming in osteoclasts. Semin Immunopathol 2019; 41(5):565–72 [eng].
[63] Jin Z, Li X, Wan Y. Minireview: nuclear receptor regulation of osteoclast and bone remodeling. Mol Endocrinol 2015;29(2):172–86 [eng].
[64] Mojsiewicz-Pieńkowska K, Jamrógiewicz M, Szymkowska K, Krenczkowska D. Direct human contact with siloxanes (silicones) - safety or risk Part 1. Characteristics of siloxanes (silicones). Front Pharmacol 2016;7:132 [eng].
[65] Chang YM, Chang HH, Tsai CC, Lin HJ, Ho TJ, Ye CX, et al. Alpinia oxyphylla Miq. fruit extract activates IGFR-PI3K/Akt signaling to induce Schwann cell proliferation and sciatic nerve regeneration. BMC Compl Alternative Med 2017;17(1):184 [eng].
[66] Liao CF, Hsu ST, Chen CC, Yao CH, Lin JH, Chen YH, et al. Effects of electrical stimulation on peripheral nerve regeneration in a silicone rubber conduit in taxol-treated rats. Materials 2020;13(5) [eng].
[67] Liao CF, Chen CC, Lu YW, Yao CH, Lin JH, Way TD, et al. Effects of endogenous inflammation signals elicited by nerve growth factor, interferon-γ, and interleukin-4 on peripheral nerve regeneration. J Biol Eng 2019;13:86 [eng].
[68] Lin YC, Kao CH, Chen CC, Ke CJ, Yao CH, Chen YS. Time-course effect of electrical stimulation on nerve regeneration of diabetic rats. PLoS One 2015;10(2):e0116711 [eng].
[69] Wang W, Huang CY, Tsai FJ, Tsai CC, Yao CH, Chen YS. Growth-promoting effects of quercetin on peripheral nerves in rats. Int J Artif Organs 2011;34(11):1095–105 [eng].
[70] Aghajanian S, Taghi Doulabi A, Akhbari M, Shams A. Facial nerve regeneration using silicone conduits filled with ammonia-functionalized graphene oxide and frankincense-embedded hydrogel. Inflamm Regen 2021;41(1):13 [eng].
[71] Gu J, Xu H, Xu YP, Liu HH, Lang JT, Chen XP, et al. Olfactory ensheathing cells promote nerve regeneration and functional recovery after facial nerve defects. Neural Regen Res 2019;14(1):124–31 [eng].
[72] Matsumine H, Numakura K, Climov M, Watanabe Y, Giatsidis G, Orgill DP. Facial-nerve regeneration ability of a hybrid artificial nerve conduit containing uncultured adipose-derived stromal vascular fraction: an experimental study. Microsurgery 2017;37(7):808–18 [eng].
[73] Spector JG, Lee P, Derby A, Roufa DG. Comparison of rabbit facial nerve regeneration in nerve growth factor-containing silicone tubes to that in autologous neural grafts. Ann Otol Rhinol Laryngol 1995;104(11):875–85 [eng].
[74] Mohammadi R, Sanaei N, Ahsan S, Masoumi-Verki M, Khadir F, Mokarizadeh A. Stromal vascular fraction combined with silicone rubber chamber improves sciatic nerve regeneration in diabetes. Chin J Traumatol 2015;18(4):212–8 [eng].
[75] Ferretti C, Rikhotso E, Muthray E, Reyneke J. Interim reconstruction and space maintenance of mandibular continuity defects preceding definitive osseous reconstruction. Br J Oral Maxillofac Surg 2013;51(4):319–25 [eng].

[76] Kim YH, Lee CH, Kim CH, Son DW, Lee SW, Song GS, et al. Clinical efficacy and safety of silicone elastomer sheet during decompressive craniectomy: anti-adhesive role in cranioplasty. Brain Sci 2021;11(1) [eng].
[77] Morgan EF, Giacomo A, Gerstenfeld LC. Overview of skeletal repair (fracture healing and its assessment). Methods Mol Biol 2021;2230:17–37 [eng].
[78] Richards CJ, Graf Jr KW, Mashru RP. The effect of opioids, alcohol, and nonsteroidal anti-inflammatory drugs on fracture union. Orthop Clin N Am 2017; 48(4):433–43 [eng].
[79] Debnath S, Yallowitz AR, McCormick J, Lalani S, Zhang T, Xu R, et al. Discovery of a periosteal stem cell mediating intramembranous bone formation. Nature 2018; 562(7725):133–9 [eng].
[80] Tsukasaki M, Komatsu N, Negishi-Koga T, Huynh NC, Muro R, Ando Y, et al. Periosteal stem cells control growth plate stem cells during postnatal skeletal growth. Nat Commun 2022;13(1):4166 [eng].
[81] Jeffery EC, Mann TLA, Pool JA, Zhao Z, Morrison SJ. Bone marrow and periosteal skeletal stem/progenitor cells make distinct contributions to bone maintenance and repair. Cell Stem Cell 2022;29(11):1547–61. e6. [eng].
[82] Bragdon BC, Bahney CS. Origin of reparative stem cells in fracture healing. Curr Osteoporos Rep 2018;16(4):490–503 [eng].
[83] Zhang H, Zhou Y, Yu N, Ma H, Wang K, Liu J, et al. Construction of vascularized tissue-engineered bone with polylysine-modified coral hydroxyapatite and a double cell-sheet complex to repair a large radius bone defect in rabbits. Acta Biomater 2019;91:82–98 [eng].
[84] You Q, Lu M, Li Z, Zhou Y, Tu C. Cell sheet technology as an engineering-based approach to bone regeneration. Int J Nanomed 2022;17:6491–511 [eng].
[85] Schell H, Duda GN, Peters A, Tsitsilonis S, Johnson KA, Schmidt-Bleek K. The haematoma and its role in bone healing. J Exp Orthop 2017;4(1):5 [eng].
[86] Xu J, Wang J, Chen X, Li Y, Mi J, Qin L. The effects of calcitonin gene-related peptide on bone homeostasis and regeneration. Curr Osteoporos Rep 2020;18(6): 621–32 [eng].
[87] Zhu WY, Guo J, Yang WF, Tao ZY, Lan X, Wang L, et al. Biodegradable magnesium implant enhances angiogenesis and alleviates medication-related osteonecrosis of the jaw in rats. J Orthop Translat 2022;33:153–61 [eng].
[88] Zhang Y, Xu J, Ruan YC, Yu MK, O'Laughlin M, Wise H, et al. Implant-derived magnesium induces local neuronal production of CGRP to improve bone-fracture healing in rats. Nat Med 2016;22(10):1160–9 [eng].